JACS
JOURNAL OF THE AMERICAN CHEMICAL SOCIETY
pubs.acs.org/JACS
Article

Silica-Supported Organolanthanum Catalysts for C−O Bond Cleavage in Epoxides

Zhuoran Wang,[§] Smita Patnaik,[§] Naresh Eedugurala, J. Sebastián Manzano, Igor I. Slowing, Takeshi Kobayashi, Aaron D. Sadow,* and Marek Pruski*

Cite This: J. Am. Chem. Soc. 2020, 142, 2935−2947
Read Online
ACCESS | Metrics & More | Article Recommendations | Supporting Information

ABSTRACT: Single-site organolanthanum complexes supported on mesoporous silica nanoparticles, La{C(SiHMe$_2$)$_3$}$_n$@MSNs, catalyze the ring-opening hydroboration reaction of aliphatic and styrenic epoxides with pinacolborane (HBpin). The surface-bound complexes, synthesized by reaction of the homoleptic tris(alkyl)-lanthanum La{C(SiHMe$_2$)$_3$}$_3$ and SBA-type MSN treated at 700 °C (MSN$_{700}$), are mostly monopodal ≡SiO—La{C(SiHMe$_2$)$_3$}$_2$ and contain an average of one bridging La←H—Si per alkyl ligand. This structure was established through a combination of solid-state NMR (SSNMR) experiments, including *J*-resolved SiH coupling and quantitative ^{29}Si measurements, diffuse reflectance IR, and elemental analysis. These rigorous analyses also established that grafting reactions in pentane provide a preponderance of ≡SiO—La{C(SiHMe$_2$)$_3$}$_2$ sites and are superior to those in benzene and THF, and that grafting onto MSN treated at 550 °C (MSN$_{550}$) results in a mixture of surface species. The single-site supported catalysts are more selective and in most cases more active than the homogeneous analogue, allow easy purification of products from the catalyst, are strongly resistant to leaching into solution phase, and may be recycled for reuse at least five times. After reaction of La{C(SiHMe$_2$)$_3$}$_n$@MSN and HBpin, species including ≡SiO—La{C(SiHMe$_2$)$_3$}(H$_2$Bpin) and ≡SiO—La{C(SiHMe$_2$)$_3$}{κ^2−pinB−O(CMe$_2$)$_2$OBH$_3$} are identified by detailed 1D and 2D ^{11}B SSNMR experiments.

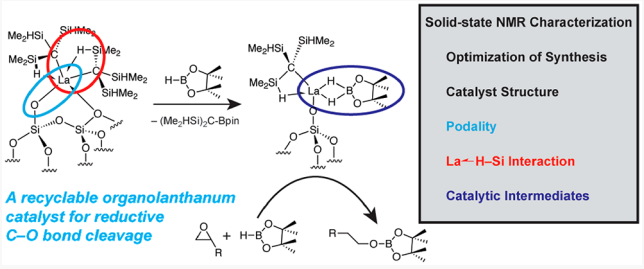

INTRODUCTION

The bond-activating properties of organolanthanides, which are well-known to readily break and form C−H and C−C bonds,[1−3] hold promise for new catalytic transformations that complement mechanisms and selectivity of transition-metal-catalyzed reactions.[4−8] Lanthanide oxophilicity can also enable C−O bond cleavage in ethers or in transesterification reactions; however, reductive catalytic C−O bond cleavage processes are typically inhibited by the stabilization of intermediates containing Ln−O bonds (Ln = lanthanides and group 3). A few examples of hydroboration of ketones and aldehydes, using the homoleptic lanthanum catalysts La{N(SiMe$_3$)$_2$}$_3$ and Cp$_3$La,[9−11] or hydroboration and C−O bond cleavage of esters catalyzed by La{C(SiHMe$_2$)$_3$}$_3$ or La{N(SiMe$_3$)$_2$}$_3$,[12,13] suggest strategies for overcoming the Ln−O bond strength to make use of highly electrophilic lanthanide centers. In fact, La{C(SiHMe$_2$)$_3$}$_3$ represents the most active and versatile catalyst for the ring-opening hydroboration of epoxides to date.[12,14,15] We note that a related approach to breaking strong M−O bonds of oxophilic sites is enabled by redox-active metal centers, for example, with Ti complexes under homogeneous conditions,[16,17] or in metal−organic frameworks (MOFs),[18] as well as Ce-containing MOF-catalyzed hydroboration of alkenes and pyridines.[19]

The oxophilic lanthanide centers also form strong bonds to oxygen in metal oxides, which is a useful property for attaching these sites onto supports in heterogeneous catalysts.[20−29] Homoleptic compounds in particular, such as La(CH$_2$Ph)$_3$THF$_3$ or La{CH(SiMe$_3$)$_2$}$_3$,[30,31] have potential in surface organometallic chemistry (SOMC).[26,32] For example, lanthanum benzyl grafted onto silica is a catalyst for styrene and ethylene polymerization and alkyne dimerization.[32] Unfortunately, the molecular precursors are limited by their typically difficult syntheses, tendency to tightly coordinate donors, such as THF or Cl as LiCl adducts, and thermal lability. These properties are exacerbated in the large, early lanthanides (i.e., La, Ce, Pr, Nd). Moreover, the combination of highly electrophilic rare-earth centers and reducing alkyl ligands results in polar Ln−C bonds that can undergo side reactions with siloxane linkages on silica to dealkylate and deactivate organolanthanide sites in SOMC. Such reactions are difficult to trace in surface species as a result of limited spectroscopic signatures of the homoleptic precursors. In

Received: October 28, 2019
Published: January 12, 2020

https://dx.doi.org/10.1021/jacs.9b11606
J. Am. Chem. Soc. 2020, 142, 2935−2947

addition, the lanthanide centers that mediate cleavage of C−O bonds, such as the reaction which occurs during the catalytic hydroboration of epoxides, might also readily break the Si−O bonds that link the organometallic species to the surface.

In contrast to benzyl and trimethylsilyl compounds, the new class of homoleptic compounds $Ln\{C(SiHMe_2)_3\}_3$ benefit from rich infrared and NMR spectroscopic features associated with the silicon-hydride moiety.[33,34] The $^1J_{SiH}$ of 137 Hz for $La\{C(SiHMe_2)_3\}_3$, measured at room temperature, corresponds to the mean of exchanging bridging La←H−Si ($^1J_{SiH}$ = 114 Hz) and nonbridging SiH ($^1J_{SiH}$ = 186 Hz), which are resolved to a 2:1 ratio at −94 °C. These properties have been useful in studying grafting reactions of disilazido compounds such as $Ln\{N(SiHMe_2)_2\}_3THF_n$ or $Ln\{N(SiHMe_2)tBu\}_3$ (with Ln = Y and Sc), which also contain bridging Ln←H−Si structures.[20,22] In $Y\{N(SiHMe_2)tBu\}_3$, for example, the averaged $^1J_{SiH}$ value responds to the presence (145 Hz) or absence (124 Hz) of a THF ligand; the value in the THF-free silica-grafted surface species (141 Hz) suggests an additional interaction with surface siloxane as a 2 e^- donor.[29] Thus, the NMR properties of SiH groups in the lanthanide alkyl species $Ln\{C(SiHMe_2)_3\}_3$ might also facilitate assignment of surface structures formed in grafting reactions.

In the present study, we have pursued the thermally stable, easily synthesized compound $La\{C(SiHMe_2)_3\}_3$ as a reactant for producing organolanthanum compounds in SOMC on mesoporous silica nanoparticles (MSNs). We report on the synthesis and structure of MSN-grafted $La\{C(SiHMe_2)_3\}_3$, and on the improved per-site catalytic activity, selectivity, and recyclability of this material compared to its soluble precursor for ring-opening hydroboration of epoxides. Among the analytical techniques capable of probing the grafting process, as well as the structures and dynamics of surface-attached organometallic species, nuclear magnetic resonance (NMR) spectroscopy proved to be particularly powerful.[29,32,35−41] Here, definitive structural characterizations of the surface-grafted alkyl lanthanum species were obtained from one- and two-dimensional (1D and 2D) solid-state (SS)NMR measurements on ^{1}H, ^{11}B, ^{13}C, and ^{29}Si nuclei, performed in concert with solution-state NMR, elemental analysis, and diffuse reflectance infrared spectroscopy (DRIFTS). Importantly, SSNMR experiments were used to understand and optimize the grafting reactions, to provide spectroscopic signatures of the secondary La←H−Si interactions in the grafted species, and to propose the structures of the active catalytic centers generated by reacting pinacolborane (HBpin) with surface-attached alkyl lanthanum species.

METHODS AND MATERIALS

Synthesis of Materials. $La\{C(SiHMe_2)_3\}_3$ was prepared by reaction of LaI_3 and $KC(SiHMe_2)_3$,[34] SBA-type MSNs were prepared by P104-templated condensation of tetramethyl orthosilicate (TMOS) under acidic conditions.[42] The silica surface was partially dehydroxylated by heating under dynamic vacuum (1 mTorr) at 550 °C (MSN_{550}) or 700 °C (MSN_{700}) for 12 h. The surface areas and pore sizes, determined by N_2 sorption, are 441 m^2/g and 9.1 nm for MSN_{550}, and 409 m^2/g and 9.1 nm for MSN_{700} (see Table S1 in the Supporting Information, which includes additional textural properties of both samples). The TEM images of MSN_{700}, shown in Figure S2 in the Supporting Information, further demonstrate the stability of the MSN structure upon thermal treatment *in vacuo*. Titration of surface silanols with $Mg(CH_2Ph)_2(O_2C_4H_8)_2$ revealed 0.75 mmol/g for MSN_{550} and 0.62 mmol/g for MSN_{700}.[43]

SSNMR Spectroscopy. SSNMR experiments were performed on a 600 MHz (14.1 T) Varian NMR spectrometer, equipped with 1.6 and 3.2 mm magic angle spinning (MAS) probes, and a 400 MHz (9.4 T) Varian NMR spectrometer, equipped with 3.2 and 5.0 mm MAS probes. 1D and 2D experiments were carried out on ^{1}H, ^{11}B, ^{13}C, and ^{29}Si nuclei and included 1D DPMAS, 1D CPMAS, 2D HETCOR and idHETCOR, 2D *J*-resolved spectroscopy,[44] and 2D MQMAS.[45] The abbreviations refer to direct polarization (DP), cross-polarization (CP), directly and indirectly detected heteronuclear correlation spectroscopy (HETCOR and idHETCOR), and multiple-quantum (MQ)MAS. The idHETCOR technique was used in combination with fast MAS to enhance the signal-to-noise ratio via the detection of ^{1}H nuclei in the direct dimension of the 2D spectrum (horizontal axis in our figures) and relegating the less sensitive nuclei, here ^{29}Si, to the indirect (vertical) dimension.[46,47] To minimize the possibility of oxygen contamination, the samples were packed in zirconia rotors in a glovebox under nitrogen atmosphere, and the experiments were carried out using nitrogen to propel the MAS rotors. The experimental details are given as needed in the text and in the figure captions, using the following symbols: B_0 is the magnetic field, ν_R the MAS rate, τ_{CP} the cross-polarization contact time to the observed nuclei, τ_{RD} the recycle delay, T_1 the longitudinal relaxation time, and AT the total acquisition time. The full sets of experimental parameters for all experiments are listed in Table S2 in the Supporting Information. The chemical shifts for ^{1}H, ^{13}C, ^{29}Si, and ^{11}B nuclei were denoted as δ and referenced according to the IUPAC recommendations.[48]

RESULTS AND DISCUSSION

Synthesis and Characterization of the Silica-Supported Organolanthanides. The homoleptic tris(alkyl) lanthanum compound $La\{C(SiHMe_2)_3\}_3$ (**1**)[33,34] and MSN_{550}[49] or MSN_{700} reacted in a rapidly stirred pentane suspension at room temperature over 20 h to give $La\{C(SiHMe_2)_3\}_n@MSN_{550}$ (**1**@MSN_{550}) or $La\{C(SiHMe_2)_3\}_n@MSN_{700}$ (**1**@MSN_{700}) and $HC(SiHMe_2)_3$ (Scheme 1). The materials **1**@MSN_{550} and **1**@MSN_{700} were characterized by mass balance of grafting, surface alcoholysis reactions, elemental analysis, as well as DRIFTS and SSNMR spectroscopy as described below.

La Loading and Podality. The La loadings and surface speciations (ratios of monopodal sites to bipodal sites, where podality is defined as the number of X-type surface silanoate ligands)[50] in **1**@MSN_{550} and **1**@MSN_{700} were evaluated by mass balance of grafting (*in situ* solution-state NMR, method I), quantification of surface alcoholysis reactions (*in situ* solution-state NMR, method II), and elemental analysis combined with quantitative ^{29}Si SSNMR (method III). The data obtained from these three methods are summarized in Table 1. In the first method, the grafting reaction performed between excess **1** and a tared quantity of MSN in benzene-d_6 was monitored by solution-state NMR, with internal standard $Si(SiMe_3)_4$ of known concentration added. The decrease in the concentration of **1** ($\mathbf{1}_{consumed}$) is proportional to the La loading, and the amount of $HC(SiHMe_2)_3$ produced ($HC(SiHMe_2)_{3-grafting}$) yields the number of Si—O—La linkages formed. With these two pieces of information, the monopodal to bipodal ratio could then be estimated assuming (1) that quantities of physiosorbed $La\{C(SiHMe_2)_3\}_3$ and (geometrically unlikely) tripodal $(\equiv Si—O)_3La$ are low with respect to the total amount of grafted lanthanum and (2) that **1** consumed by grafting at silanols produces primarily $HC(SiHMe_2)_3$. The amounts of $\mathbf{1}_{consumed}$ for both MSN_{550} and MSN_{700} grafting reactions are less than initial surface silanol loading, for reasons discussed in detail below, and **1** is not

https://dx.doi.org/10.1021/jacs.9b11606
J. Am. Chem. Soc. 2020, 142, 2935−2947

Scheme 1. Reactions of La{C(SiHMe$_2$)$_3$}$_3$ and Partially Dehydroxylated Mesoporous Silica Nanoparticles (MSNs) Previously Treated under Vacuum at 550 °C (MSN$_{550}$) or 700 °C (MSN$_{700}$)

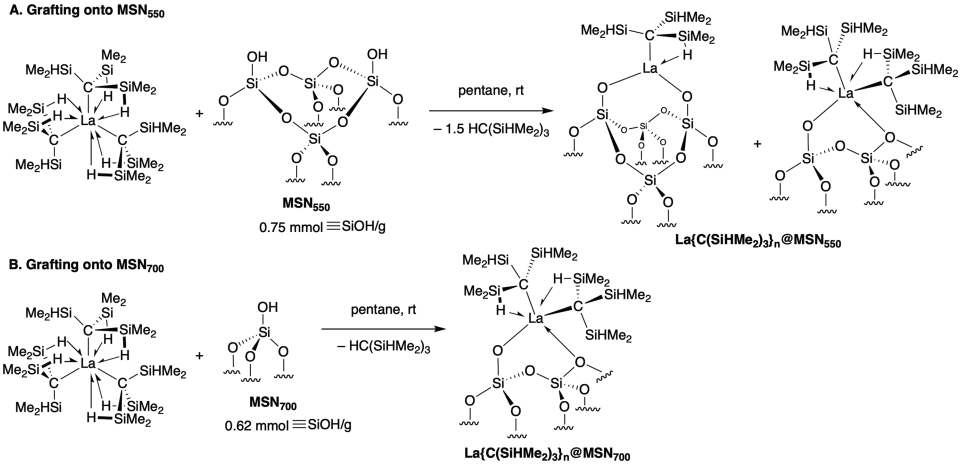

Table 1. Podalities for 1@MSN$_{550}$ and 1@MSN$_{700}$ Determined by Mass Balance of Grafting (*in Situ* Solution-State NMR), Surface Alcoholysis Reactions (*in situ* Solution-State NMR), and Elemental Analysis with Quantitative ^{29}Si SSNMR

Method		1@MSN$_{550}$	1@MSN$_{700}$
grafting mass balance (method I)	**1**$_{consumed}$ (mmol/g)	0.35	0.25
	HC(SiHMe$_2$)$_{3–grafting}$ (mmol/g)	0.55	0.27
	ratio **1**$_{consumed}$: HC(SiHMe$_2$)$_{3–grafting}$	1.0 : 1.6	1.0 : 1.1
	ratio **monopodal : bipodal**	**0.4 : 0.6**	**0.9 : 0.1**
alcoholysis quantification (method II)	**1**$_{consumed}$ (mmol/g)	0.35	0.25
	HC(SiHMe$_2$)$_{3–i\text{PrOH}}$ (mmol/g)	0.55	0.48
	ratio **1**$_{consumed}$: HC(SiHMe$_2$)$_{3–i\text{PrOH}}$	1.0 : 1.6	1.0 : 1.9
	ratio **monopodal : bipodal**	**0.6 : 0.4**	**0.9 : 0.1**
quantitative ^{29}Si SSNMR and elemental analysis (method III)	ICP-OES, La (mmol/g)	0.353	0.269
	^{29}Si DPMAS, –C(SiHMe$_2$)$_3$ (mmol/g)	0.473	0.513
	ratio La : –C(SiHMe$_2$)$_3$	1.00 : 1.34	1.00 : 1.91
	ratio **monopodal : bipodal**	**0.34 : 0.66**	**0.91 : 0.09**

detected in extracts upon washing **1**@MSN with benzene or pentane, suggesting that physiosorbed La{C(SiHMe$_2$)$_3$}$_3$, if any, is a minor component of the products. Using a complementary method II, the number of —C(SiHMe$_2$)$_3$ groups coordinating surface-attached La centers could be approximated directly by reacting isolated **1**@MSN$_{550}$ or **1**@MSN$_{700}$ with isopropyl alcohol (*i*PrOH, surface alcoholysis reaction). The podality was then deduced by comparing the produced HC(SiHMe$_2$)$_3$ (HC(SiHMe$_2$)$_{3–i\text{PrOH}}$) with the La loading obtained from the mass balance experiment. With method III, the La loading and the number of —C(SiHMe$_2$)$_3$ groups coordinating surface-bound La centers were independently determined using elemental analysis (ICP-OES) and quantitative ^{29}Si SSNMR measurements, providing alternative measurements for calculating the average podality. As can be seen from the good agreement in results from methods I–III in Table 1, 90% of surface species in **1**@MSN$_{700}$ are monopodal dialkyl sites of the type ≡Si—O—La{C(SiHMe$_2$)$_3$}$_2$. In contrast, **1**@MSN$_{550}$ is a mixture of surface species, most likely monopodal and bipodal ((≡Si—O—)$_2$LaC(SiHMe$_2$)$_3$) in an approximately 1:1 ratio. The minor deviation between estimated podality in MSN$_{550}$ for the three methods could be attributed to side dehydrocoupling and SiH/SiC redistribution reactions involving —C(SiHMe$_2$)$_3$ and surface SiOH groups, exacerbated in benzene solvent needed for method I, whereas the sample for method II is prepared in pentane (see below), which increased the amount of HC(SiHMe$_2$)$_3$ released during alcoholysis reactions. Additional inaccuracies of methods I and II may arise due to the reactions of HC(SiHMe$_2$)$_3$ with the silica surface, which were indicated by the ^{13}C CPMAS spectra discussed below.

Note that the La loadings on MSN$_{550}$ and MSN$_{700}$ are relatively similar, 0.35 and 0.27 mmol/g, respectively. From the amounts of Si–O–La linkages formed (see Scheme 1 and Table 1) and the titration results of the silica surface, it follows that the fractions of surface SiOH groups consumed by grafting in these two samples were about 73% and 44%. It is clear that, at a lower calcination temperature of MSN, the bipodal form is preferable and accounts for 60–70% of all La metal centers. Evidently, partially dehydroxylating the MSN at higher temperature, which primarily reduces the number of vicinal silanol groups, prevents the formation of bipodal sites with only a minor effect on La loading.

https://dx.doi.org/10.1021/jacs.9b11606
J. Am. Chem. Soc. 2020, 142, 2935–2947

The "incomplete consumption" of the SiOH groups is primarily due to the bulky size of **1**, which limits the surface site density ($La\{C(SiHMe_2)_3\}_n$@MSN_{550}, 0.48 La per nm^2; $La\{C(SiHMe_2)_3\}_n$@MSN_{700}, 0.37 La per nm^2; see Figure 1),

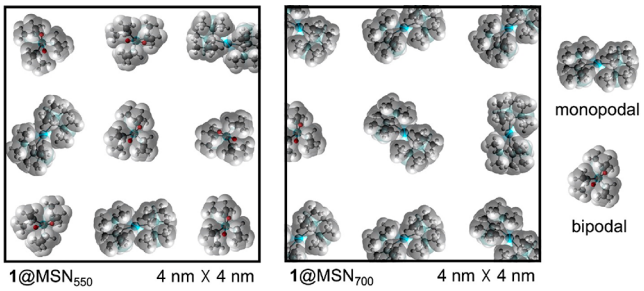

Figure 1. Surface coverage model of $La\{C(SiHMe_2)_3\}_n$@MSN. Note that the presented scheme does not account for pore curvature.

rendering a fraction of silanols inaccessible. Second, the ^{13}C CPMAS and ^{29}Si CPMAS spectra (Figure 2B–E and Figure S9 in the Supporting Information), discussed in detail later in this paper, show that some of the accessible SiOH groups were taken up by the products of side reactions with the $HC(SiHMe_2)_3$ ligands released during grafting. Third, a non-negligible fraction of SiOH groups may reside in inaccessible micropores in the SBA. Although the nitrogen sorption isotherms (see Figure S1 in the Supporting Information) showed the presence of micropores in MSN_{550} and MSN_{700}, at less than 1.5% and 0.5% of the total pore volume, respectively, these sites are difficult to quantify. The exact diameters of micropores are not known, except that they are smaller than 2 nm, and some may be off-limits also to the titrating molecules ($Mg(CH_2Ph)_2(O_2C_4H_8)_2$). However, even with the surface-to-volume ratio being higher in small-diameter pores, their SiOH content is unlikely to exceed a few %. Lastly, we considered another hypothesis that could explain the presence of unreacted SiOH groups, namely, clogging of the pore entrances with the initially grafted species. However, we found the pore-clogging scenario to be unlikely for two reasons. First, the mesopores have a uniform pore size of ~9.1 nm (see Figure S1 in the Supporting Information), which is much wider than the molecular size of the grafted species (ca. 1.2 nm). A densely packed monolayer of monopodal species would only decrease the effective pore diameter to ca. 6.5 nm, which would not block intrapore diffusion. Second, the STEM images and EDX spectroscopy mapping showed a homoge-

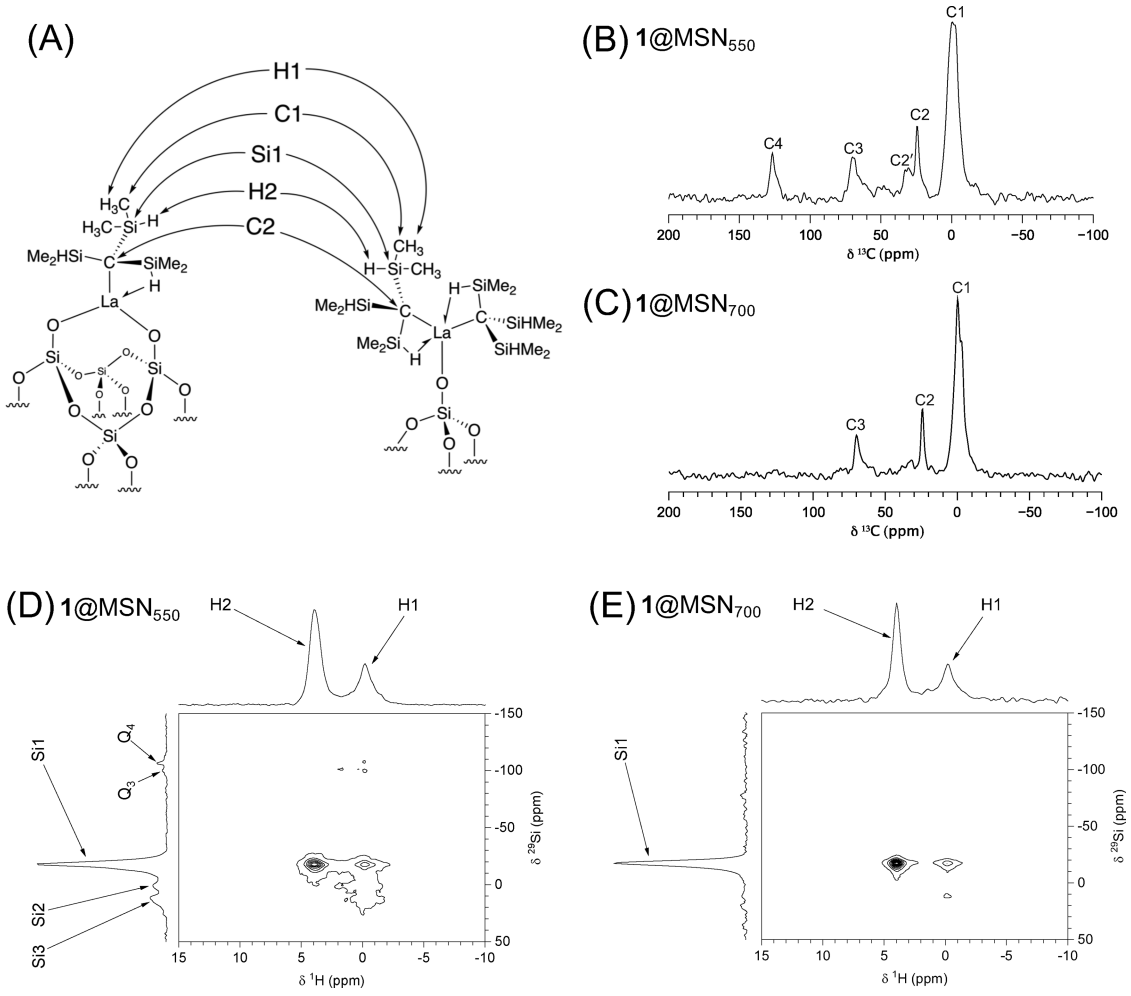

Figure 2. (A) Bipodal and monopodal structures of **1**@MSN with peak assignments. (B, C) ^{13}C CPMAS spectra of **1**@MSN_{550} and **1**@MSN_{700}; (D, E) $^{1}H\{^{29}Si\}$ idHETCOR spectra of **1**@MSN_{550} and **1**@MSN_{700}; all grafted in pentane. Experimental conditions: B_0 = 9.4 T, ν_R = 8 kHz (B, C) and 18 kHz (D, E), τ_{CP} = 2 ms (B, C) and 4 ms (D, E), and AT = 3.1 h (B, C) and 25.5 h (D, E). A more detailed list of parameters is given in the Supporting Information.

https://dx.doi.org/10.1021/jacs.9b11606
J. Am. Chem. Soc. 2020, 142, 2935–2947

neous distribution of La over the MSN (see Figure S3 in the Supporting Information).

Surface Infrared Spectroscopy. The DRIFTS spectra of isolated **1**@MSN_{550} and **1**@MSN_{700} are very similar and suggest that both samples contain organometallic species (see Figure S4 in the Supporting Information). The most notable features are bands at 2108 and 1864 cm^{-1}, which are assigned to ν_{SiH} of terminal SiH and bridging La←H—Si moieties, respectively, in organometallic surface species. These assignments are aided by similar bands at 2110 and 1829 cm^{-1} in the corresponding spectrum of **1**, and supported by Hessian calculations of an energy-minimized gas-phase structure and the comparable solid-state structure determined by single-crystal X-ray diffraction.[34] The DRIFTS spectra indicate that at least some of the secondary interactions in **1** are also present after grafting reactions replace one or two —$C(SiHMe_2)_3$ ligands with ≡Si—O—La linkages to the silica surface. The frequency of the La←H—Si band in **1**@MSN is higher than the corresponding signal in **1**, which may reflect a higher ratio of H—Si to La←H—Si in the surface species (see $^1J_{SiH}$ discussion below).

SSNMR: Basic Structures of 1@MSN_{550} and 1@MSN_{700}. The ^{13}C CPMAS and $^1H\{^{29}Si\}$ idHETCOR spectra of **1**@MSN_{550} and **1**@MSN_{700} grafted in pentane are shown in Figure 2, along with the corresponding schematic structures and site assignments. The ^1H, ^{13}C, and ^{29}Si chemical shifts, which are all attributable to silica-bound species, are listed in Table 2. The resonances labeled H1, H2, C1, C2, and Si1 can be assigned to **1**@MSN (Figure 2A), based on the chemical shift values reported for **1** by solution-state NMR.[34] Note that C2 is represented by a single line in **1**@MSN_{550} and **1**@MSN_{700}, whereas the resonance assigned to C1 consists of at least two partly overlapping components, which is more evident in the spectrum of **1**@MSN_{700} (Figure 2C). The C1 line shape reflects the conformational differences between the ligands due to interactions with the silica surface within the pores but also includes resonances from ligands released during grafting and subsequently bound to the silica surface (*vide infra*). As expected, the dominant Si1 peak at −18 ppm, observed in the $^1H\{^{29}Si\}$ idHETCOR spectra in Figure 2D,E, correlates strongly with H2 and relatively weakly with H1, which further confirms the assignments of H1, H2, and Si1 (note that there is one H2 atom per 6 methyl H1s, but the latter are two bonds away and undergo rapid rotations which hinder the polarization transfers).

Table 2. Summary of Observed ^1H, ^{13}C, and ^{29}Si Resonances and Their Corresponding Assignments

resonance	chemical shift[a] (δ, ppm)	chemical shift[b−e] (δ, ppm)	assignment
H1	−0.1	0.4[b]	−SiH(CH_3)$_2$
H2	3.9	4.3[b]	−Si**H**(CH_3)$_2$
C1	−1	3.6[b]	−SiH(CH_3)$_2$
C2	24	31.8[b]	−**C**($SiHMe_2$)$_3$
C2′	30	N.A.[c]	La−**C**($SiHMe_2$)$SiMe_2$O−[d]
C3	70	68.0[d]	(−O)**C**($SiHMe_2$)$_3$[d]
C4	127	122.5[d]	(−O)$_2$**C**($SiHMe_2$)$_2$[d]
Si1	−18	−18.5[b]	−OLa{C(**Si**HMe_2)$_3$}$_n$
Si2	1	0.0[e]	−O**Si**HMe_2
Si3	11	12.0[e]	−O**Si**Me_3[f]

[a]The chemical shifts observed in SSNMR experiments. The ^{29}Si resonances associated with the silica support, corresponding to Q^n sites described by a general formula $(\equiv SiO)_n\mathbf{Si}(OH)_{4-n}$, are not included. [b]The chemical shifts reported for **1** by solution-state NMR.[34] [c]N.A.: not available. [d]The corresponding structures and chemical shift values obtained from DFT calculations are included in the Supporting Information. [e]The chemical shifts were reported by Tuel et al.[51] [f]This peak may also include a minor contribution from Si in dehydrocoupled alkyl ligand in **1**@MSN_{550} (see Scheme S1 in the Supporting Information).

Minor Organic Surface Species. In the following we discuss the possible origins of weaker resonances representing carbons C2′, C3, and C4 (observed at ∼30, ∼70, and ∼127 ppm), as well as silicons Si2 and Si3 (observed at ∼1 and ∼11 ppm). Based on the ^{13}C CPMAS measurements on MSN_{550} and MSN_{700} supports, which did not yield any discernible ^{13}C signals, we can conclude that all peaks observed in **1**@MSN represent species originating from grafted groups. The most plausible assignment of the weakest resonance labeled C2′ is to the C2 carbon in the La-bound ligand that underwent the Si−H/SiOH dehydrocoupling reaction (see Scheme S1 in the Supporting Information). To assign C3 and C4, we considered the surface-bound species (−O)$C(SiHMe_2)_3$ and (−O)$_2$C-$(SiHMe_2)_2$, respectively, resulting from La-mediated alkoxylation on the surface with −$C(SiHMe_2)_3$ ligands. To support these assignments, we carried out DFT calculations of ^{13}C and ^{29}Si chemical shifts for both structures; the calculation details and corresponding structures are given in the Supporting Information (Figures S5 and S6). The ^{13}C shifts calculated for the surface-bound carbons in (−O)$C(SiHMe_2)_3$ and (−O)$_2$C-$(SiHMe_2)_2$ species agree well with the experimental values for C3 and C4, whereas the ^{29}Si chemical shift values coincide with the peak labeled Si2 in Figure 2D. The appearance of the surface (−O)−C linkage, however, is surprising under our oxidant-free grafting conditions and contrasts the typical nucleophilic behavior of the −$C(SiHMe_2)_3$ ligand. Nonetheless, these surface alkoxides are also most plausible, considering the moieties present in the reaction mixture during grafting and ^{13}C NMR chemical shifts, and we are currently investigating related reactions to better understand the mechanism of this result.

Additional information about the minor silica-bound species was obtained from the $^1H\{^{29}Si\}$ idHETCOR spectra in Figure 2D,E. Here, the signal Si3 is assigned to −$OSiMe_3$ species formed according to Scheme S2 in the Supporting Information, where the intermediate species −$OSiHMe_2$ may further contribute to the previously discussed Si2 peak. These assignments are based on reported chemical shifts,[51] the observed $^1H-^{29}Si$ correlations being Si2−H1, Si2−H2, and Si3−H1 (see Figure 2D), and a chemical shift anisotropy (CSA) recoupling experiment[52] that revealed asymmetric and axially symmetric CSA for Si2 and Si3, respectively. The organo-rare-earth compounds, particularly hydrides, are known to catalyze redistribution of organosilanes via Si−C bond cleavage steps,[53,54] and these reactions catalyzed by solution-phase **1** or grafted **1**@MSN may indeed produce the additional surface silyl species depicted in Scheme S2. Note that $HC(SiHMe_2)_3$ is not capable of silylating or alkylating the bare MSN_{550} surface, as demonstrated by the spectrum in Figure S7 in the Supporting Information.

To summarize the analysis of the "unwanted" surface species, we point out that our study provided several important insights. First, guided by the above results, we were able to optimize the grafting process such that it led to deposition of

https://dx.doi.org/10.1021/jacs.9b11606
J. Am. Chem. Soc. 2020, 142, 2935−2947

the desired organolanthanum complexes with minimum pollution by the side reactions, as detailed in the next section. Second, the reactions of $HC(SiHMe_2)_3$ with the surface were not extensive enough to affect the podality estimates by methods I and II, which agreed well with method III. Lastly, none of the species appeared to be active in the catalyst generated by reacting **1**@MSN with HBpin. To substantiate this claim, we note that the ^{13}C CPMAS spectrum of **1**@MSN_{550}+HBpin contained all the three peaks attributed to C2′, C3, and C4 (see Figure S8 in the Supporting Information).

Optimization of the Synthesis Guided by SSNMR. Our SSNMR analysis of **1**@MSNs shows that the grafting process is influenced by the silica pretreatment temperature and the solvent. By comparing Figure 2B with Figure 2C and Figure 2D with Figure 2E, it is clear that the treatment of MSN at 700 °C under vacuum leads to "cleaner" deposition of the desired structures depicted in Figure 2A. Indeed, the ^{13}C peaks at 30 and 127 ppm present in the ^{13}C CPMAS spectrum of **1**@MSN_{550} were not observed in **1**@MSN_{700}. More importantly, grafting on MSN_{700} suppressed the surface side reactions, yielding only the Si1 resonance in the $^1H\{^{29}Si\}$ idHETCOR spectrum of Figure 2E. The 1D ^{29}Si CPMAS spectra further confirmed this result (see Figure S9 in the Supporting Information). In the grafting of **1** on MSN_{700}, ^{29}Si NMR data also rule out reactions involving highly strained siloxanes present in MSN_{700}.[55]

The ^{29}Si CPMAS spectra of samples grafted in pentane, THF, and benzene (Figure 3) demonstrated that the loading of

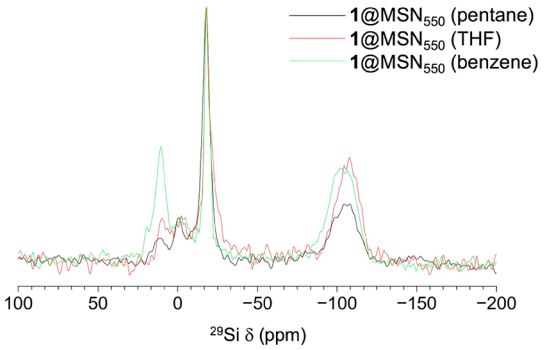

Figure 3. ^{29}Si CPMAS spectra of **1**@MSN_{550} grafted in different solvents. The signal intensities are normalized with respect to the Si1 peak height. Experimental conditions: B_0 = 9.4 T, ν_R = 18 kHz, τ_{CP} = 4 ms, and AT = 6.4 h. A more detailed list of parameters is given in the Supporting Information.

1 and surface silylation are both strongly influenced by the solvent used during the grafting process. Clearly, pentane exhibited the best performance among the solvents tested; not only was the integrated spectral intensity of Si1 per unit mass of sample more than doubled compared to THF and benzene (Table 3), but the surface silylation was significantly suppressed. As implied above, the surface silylation and CH/SiOH dehydrocoupling reactions of the $HC(SiHMe_2)_3$ product of grafting are catalyzed by lanthanum, and these reactions, which compete with $La\{C(SiHMe_2)_3\}_3$ grafting, are apparently faster in THF and benzene.

SSNMR: Secondary La←H−Si Interactions. The DRIFTS spectra of **1**@MSN discussed above suggested that secondary interactions of the type La←H−Si were also present on the surface. Similarly to our earlier study of MSN-grafted

Table 3. Integrated Si1 Peak Intensities in ^{29}Si CPMAS Spectra for 1@MSN_{550} Grafted in Different Solvents

solvent used in grafting process	integrated intensity of Si1 peak[a]
pentane	9.52
THF	4.09
benzene	3.99

[a]The peak intensity is normalized to the mass.

$Y\{N(SiHMe_2)tBu\}_3$,[29] we acquired the 2D *J*-resolved ^{29}Si SSNMR[44] spectra to obtain additional signatures of such interactions in **1**@MSN_{550} and **1**@MSN_{700}. Two traces of 2D spectra projected along the $^1J_{SiH}$ dimension at Si1 position are shown in Figure 4. After proper rescaling, the $^1J_{SiH}$ values for

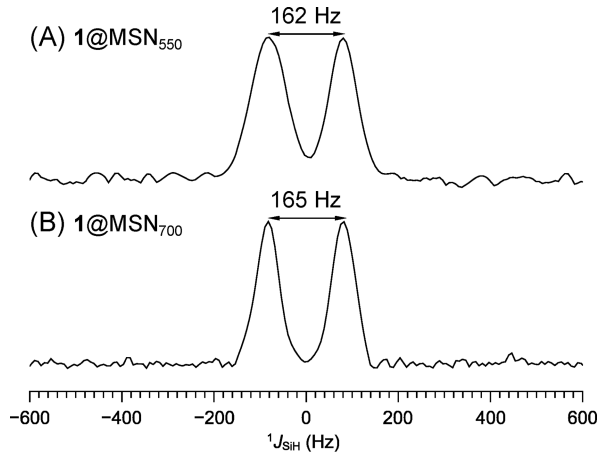

Figure 4. $^1J_{SiH}$ doublets (scale corrected) extracted for Si1 from the 2D *J*-resolved spectra of (A) **1**@MSN_{550} and (B) **1**@MSN_{700}. The spectra were acquired using the pulse scheme reported by Lesage et al.,[44] with phase-modulated Lee−Goldburg (PMLG)[56] $^1H-^1H$ homonuclear decoupling during the evolution time. The scaling factor was determined to be 0.41 by experimentally measuring the ^{29}Si *J*-splitting of (4-methoxyphenyl)-phenyl silane. Experimental conditions: B_0 = 14.1 T, ν_R = 15 kHz, τ_{CP} = 4 ms, and AT = 30 h. A more detailed list of parameters is given in the Supporting Information.

1@MSN_{550} and **1**@MSN_{700} are equal to 162 and 165 Hz, respectively. These couplings are smaller than the 186 Hz value associated with the 2-center−2-electron (2c−2e) Si−H bond and larger than the 114 Hz value that characterizes the La←H−Si 3-center−2-electron (3c−2e) interaction. However, they agree very well with the average $^1J_{SiH}$ value of 1/3(2 × 186 + 114) = 162 Hz, corresponding to two Si−H and one La←H−Si configurations undergoing fast exchange. For comparison, the averaged $^1J_{SiH}$ value for two La←H−Si and one Si−H configurations matches the experimental value of 137 Hz for **1**, which indeed contains two La←H−Si interactions per every $-C(SiHMe_2)_3$ ligand.[34] Thus, we confirm that there is indeed one La←H−Si interaction per every $-C(SiHMe_2)_3$ ligand in **1**@MSN. Fewer secondary interactions in **1**@MSN are somewhat unexpected because a coordinatively unsaturated, monopodal La center on the silica surface should be highly electrophilic. Instead, we propose that the metal center is stabilized by the coordination of an oxygen in a surface siloxane to satisfy the coordination sphere.

Catalytic Hydroboration of Epoxides with HBpin Using 1@MSNs. Both materials **1**@MSN_{550} and **1**@MSN_{700} proved to be effective precatalysts at 5 mol % La loading (relative to epoxide) for ring-opening C−O bond cleavage of

https://dx.doi.org/10.1021/jacs.9b11606
J. Am. Chem. Soc. 2020, 142, 2935−2947

epoxides via hydroboration to give borate esters, and both performed similarly in terms of activity and product yield (Table 4). These reaction performance metrics are comparable, and often superior, to the soluble catalyst precursor $La\{C(SiHMe_2)_3\}_3$;[12] in several cases the supported catalyst out-performed the homogeneous precursor. These organolanthanide catalysts also are advantaged over the state-of-the-art transition-metal-based catalysts, which are limited to conversions of styrenyl oxides in reactions with HBpin.[14,15] Most of the catalytic hydroboration reactions proceeded at room temperature, although cyclopentene oxide required gentle heating at 60 °C for 1 day. In the absence of one of these catalysts, equivalent amounts of styrene oxide and HBpin reactants were present in solution before and after standing for 10 days at room temperature (i.e., uncatalyzed hydroboration is insignificant under these conditions). The catalysts were effective for a wide range of aliphatic- and aromatic-substituted epoxides, including 2,2-dialkyl-epoxides, cycloalkene oxides, styrene oxides, 2,3-alkyl,aryl-epoxides, stilbene oxides, and ether-substituted epoxides. The latter two types of epoxides include bromo- and chloroaryl groups, and aryl alkyl ether moieties, and these functionalities were retained in the ring-opened products. **1**@MSN_{700}-catalyzed hydroboration of halo-substituted styrene oxides occurred quantitatively at room temperature, whereas homogeneous **1** required heating. Branched products were obtained with alkyl-substituted epoxides, resulting from cleavage of the C−O bond at the less substituted position. In contrast, styrenic epoxides reacted to give linear products resulting from C−O bond cleavage at the benzylic position. C−O bond cleavage in reactions of *β*-methylstyrene oxide also occurred in the position adjacent to the phenyl. Likely, benzylic stabilization of carbon at that site affects the relative stability of the intermediates, giving selective cleavage.

Table 4. Catalytic Hydroboration Results of Epoxides with Pinacolborane Using 1@MSN_{550} and 1@MSN_{700}

Reaction[a]	Catalyst	Yield[b]
	**1**	100 (92)[c]
	1@MSN_{550}	100 (92)
	1@MSN_{700}	100
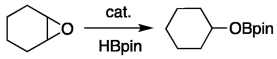	**1**	98 (85)[c]
	1@MSN_{550}	92 (88)
	1@MSN_{700}	98
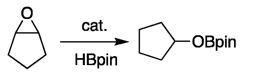	**1**	98 (78)[c]
	1@MSN_{550}	74 (65)[d]
	1@MSN_{700}	85[d]
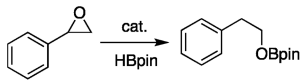	**1**	98 (95)[c]
	1@MSN_{550}	92 (90)
	1@MSN_{700}	100
	**1**	100 (98)[c]
	1@MSN_{550}	96
	1@MSN_{700}	100
	**1**	1:3[c,e]
	1@MSN_{550}	96
	1@MSN_{700}	100
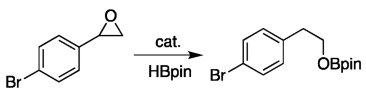	**1**	73
	1	95[f]
	1@MSN_{550}	93±1[g]
	1@MSN_{700}	100[g] (90)
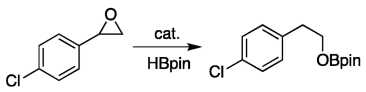	**1**	60
	1	92[f]
	1@MSN_{550}	100
	1@MSN_{700}	100 (92)
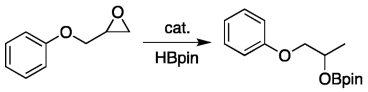	**1**	95
	1@MSN_{550}	91±1[g]
	1@MSN_{700}	97±2[g] (86)
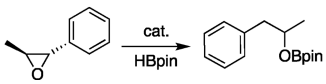	**1**	92
	1@MSN_{550}	92±2[g]
	1@MSN_{700}	87±2[g] (78)

[a]Reaction conditions: 5 mol % La (as **1**@MSN), suspended in benzene or benzene-d_6, 1.5 equiv of HBpin, r.t., 1 day. [b]NMR yield, using $Si(SiMe_3)_4$ as the internal standard; isolated (as alcohol) given in parentheses. [c]Ref 12. [d]60 °C, 1 day. [e]Obtained as a mixture of 1,2-diphenylalcohol and 2,2-diphenylalcohol. [f]60 °C, 1 h. [g]Average of three experiments.

In addition, the supported organolanthanide also provided improved selectivity in the catalytic ring-opening hydroboration of cis-stilbene oxide, giving 1,2-diphenylethanol, whereas the soluble catalyst precursor $La\{C(SiHMe_2)_3\}_3$ afforded a mixture of 1,2-diphenylethanol and a rearranged 2,2-diphenylethanol product.[12]

The catalytic activity of **1**@MSN was solely associated with the solid material, even though soluble **1** is a viable catalyst in its own right. Styrene oxide ring-opening hydroboration reactions, in which half of the supernatant solution was separated from the reaction mixture and filtered after 1 h (at ca. 35% conversion), did not undergo further conversion over 1 day, whereas the portion of solution that remained in contact with **1**@MSN fully converted to borate ester. Thus, the active sites are bonded to the surface and remain attached to the silica throughout the catalytic transformation. The La loading of the catalyst after hydroboration, analyzed by ICP-OES, was 0.260 ± 0.002 mmol/g, which is similar to the 0.269 La loading in the virgin **1**@MSN_{700} material (Table 1). Finally, the La concentration in the supernatant solution was below the ICP-OES detection limit; thus, leaching can be excluded. These data indicate that the active sites are bonded to the surface and remain attached to the silica throughout the catalytic transformation.

The solid catalytic material derived from **1**@MSN_{700} could be recovered from the reaction mixture (by centrifugation) and reused for additional hydroboration reactions. In these experiments, conversions were measured by solution-state NMR after 5 h. The conversion was equivalent after recycling the solid catalyst 3 times but was diminished by a factor of ca. 2 in the fourth and fifth cycles (Table 5). These results are remarkable, given the reducing nature of the lanthanum surface

Table 5. Recycling Experiments Run to Partial Conversion

recycle	remaining [styrene oxide] (M)	product [$PhCH_2CH_2OBpin$] (M)	conversion[a] (%)
0	0.083	0.10	55 ± 1
1	0.082	0.09	51 ± 1
2	0.082	0.09	51 ± 2
3	0.080	0.09	51 ± 2
4	0.18	0.05	25 ± 3
5	0.18	0.05	25 ± 3

[a]5 h reaction time using **1**@MSN_{700} as catalyst. Average of two sequences of recycling experiments.

https://dx.doi.org/10.1021/jacs.9b11606
J. Am. Chem. Soc. 2020, 142, 2935−2947

Scheme 2. Reaction of La{C(SiHMe$_2$)$_3$}$_n$@MSN$_{700}$ and HBpin (Surface Products Are Further Discussed below)

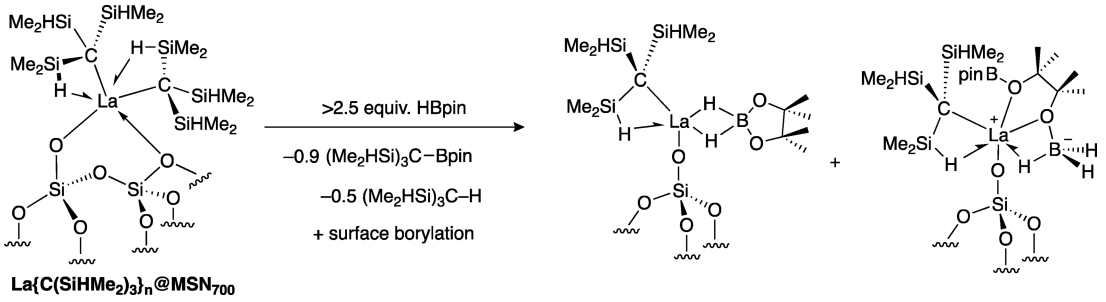

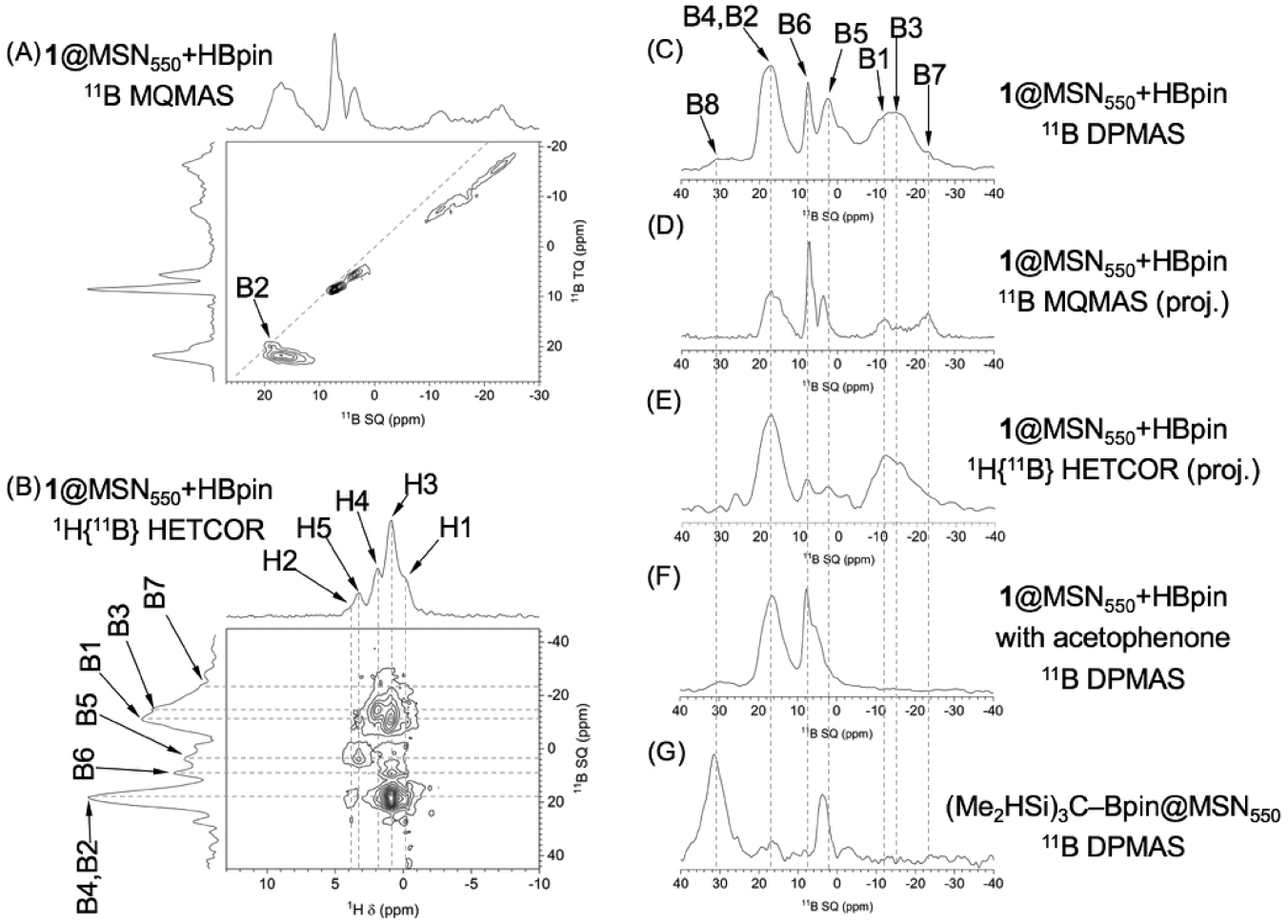

Figure 5. (A–E) ^{11}B SSNMR spectra of **1**@MSN$_{550}$+HBpin, acquired at 14.1 T, using ν_R = 36 kHz and τ_{RD} = 1 s (which is greater than 5T_1 for all sites involved). (A) *Z*-filtered MQMAS, AT = 42.7 h, dashed line denotes the so-called chemical shift axis, along which the resonances would be located in the absence of quadrupolar interactions; (B) ^{1}H{^{11}B} HETCOR, τ_{CP} = 0.2 ms and AT = 36.4 h. (C) DPMAS, AT = 2.3 h. (D) Projection of the MQMAS spectrum (in part A) along the MAS (horizontal) dimension. (E) Projection of the HETCOR spectrum (in part B) along the ^{11}B dimension. (F, G) ^{11}B DPMAS spectra of **1**@MSN$_{550}$+HBpin after reacting with acetophenone and of a reference sample (Me$_2$HSi)$_3$C–Bpin@MSN$_{550}$, respectively, both acquired with AT = 2.3 h, under otherwise the same conditions as parts A–E. A more detailed list of experimental parameters is given in the Supporting Information.

species and of HBpin. HBpin could potentially react to break ≡Si—O—La surface linkages allowing the catalyst to be leached from the surface. Leaching, as noted above, was not detected. Alternatively, strongly reducing LaH or La{H$_2$Bpin} surface species could reduce Si—O—Si linkages, giving tripodal (≡SiO)$_3$La, which would be deactivated for hydroboration. Such steps are proposed in the hydrogenolysis of ≡SiOZr(CH$_2$CMe$_3$)$_3$, which gives the tripodal (≡SiO)$_3$ZrH.[57] This latter process could occur but was sufficiently slow that catalytic activity for styrene oxide ring-opening hydroboration was equivalent over 3 recycling steps.

Characterization of Catalytic Sites in 1@MSN$_{550}$ or 1@MSN$_{700}$ after the Reaction with HBpin. *Solution-State NMR: Reaction of 1@MSN$_{700}$ with HBpin.* Reaction of 0.020 g (0.005 mmol) of **1**@MSN$_{700}$ (0.269 mmol of La/g) and 5.0 equiv of HBpin in benzene-d_6 released 0.9 equiv of (Me$_2$HSi)$_3$C–Bpin and 0.54 equiv of HC(SiHMe$_2$)$_3$ (see Scheme 2) into the solution phase. Si(SiMe$_3$)$_4$ and *n*BuBpin

https://dx.doi.org/10.1021/jacs.9b11606
J. Am. Chem. Soc. 2020, 142, 2935–2947

were used as standards for determining concentrations in solution-state ^{1}H and ^{11}B spectra, respectively. $(Me_2HSi)_3C-$Bpin was identified by ^{1}H NMR signals at 4.51, 1.00, and 0.40 ppm, and by a singlet in the ^{11}B NMR spectrum at 32 ppm. The ^{1}H NMR signals for $HC(SiHMe_2)_3$ appeared at 4.31, 0.160, and −0.85 ppm.[58] The reaction consumed 2.5 equiv of HBpin (0.012 mmol). Reactions with a larger excess of HBpin (e.g., 9 equiv) consumed and produced similar amounts of HBpin, $(Me_2HSi)_3C-$Bpin, and $HC(SiHMe_2)_3$. For comparison, **1** and HBpin reacted to give $(Me_2HSi)_3C-$Bpin and $H_nLa\{C(SiHMe_2)_3\}_{3-n}$, where the latter species was revealed as hydridic by its reaction with acetophenone to give lanthanum alkoxide [La]OCHMePh, and then hydrolyzed to the alcohol 1-phenylethanol.[12] The hydride species, however, was not directly detected by ^{1}H NMR. Moreover, we note that ^{1}H and ^{11}B NMR spectra of $H_nLa\{C(SiHMe_2)_3\}_{3-n}$ in the presence of HBpin contained signals for HBpin and $(Me_2HSi)_3C-$Bpin, whereas persistent lanthanum-pinacolborane or lanthanum pinacolborohydride adducts were not detected. Instead, these lanthanide borohydride species were postulated on the basis of kinetic experiments that revealed their transient nature in solution phase.

The formation of $HC(SiHMe_2)_3$ in the reactions of **1**@MSN_{700} and HBpin is unexpected. In order to test for the source of H in the surprising alkane product, we reacted **1**@MSN_{700} and ^{2}HBpin, which yielded $(Me_2HSi)_3C-$Bpin and $HC(SiHMe_2)_3$. $^{2}HC(SiHMe_2)_3$ was not detected in the ^{2}H NMR spectrum of the reaction mixture, whereas the spectrum of an independently prepared sample of $^{2}HC(SiHMe_2)_3$ contained a ^{2}H NMR signal at −0.93 ppm. From these observations, we propose that $HC(SiHMe_2)_3$ is formed from reactions of surface silanols and lanthanum alkyls as a result of treatment with HBpin. In particular, the unsaturated lanthanum alkyl intermediate $\equiv SiO-La(H)C(SiHMe_2)_3$ formed in the presence of HBpin could more readily react with a silanol in close proximity than bulky $\equiv SiO-La\{C(SiHMe_2)_3\}_2$.

SSNMR: Structures of 1@MSN_{550}+HBpin and 1@MSN_{700}+HBpin. The structures of catalytic centers involved in hydroboration and the associated reaction mechanisms were studied by using an array of ^{11}B SSNMR experiments, which included DPMAS, MQMAS, and $^{1}H\{^{11}B\}$ HETCOR. Because the catalysts are recyclable, without loss of activity over several experiments, the HBpin-treated **1**@MSN offers the possibility to characterize species that are most likely associated with catalytic activity. Except for the relative peak intensities, the spectra taken for **1**@MSN_{550}+HBpin and **1**@MSN_{700}+HBpin were very similar, and while only the former are shown in Figure 5, their implications are applicable to both catalysts. The DPMAS and MQMAS spectra of **1**@MSN_{700}+HBpin are shown in the Supporting Information. Overall, the ^{11}B spectra are unexpectedly complicated, featuring multiple peaks, which we labeled as B1−B8. The ^{1}H resonances in the HETCOR spectrum are labeled H1−H5, where H1 and H2 represent the previously identified hydrogen atoms in **1**@MSN_{550}. For the convenience of readers who are mainly interested in the results, we show in Table 6 the observed ^{11}B shifts, along with the proposed corresponding structures. Assigning these structures required examination of multiple spectra, as summarized below.

We first briefly explain the information content associated with different spectra in Figure 5. The DPMAS spectra of half-integer quadrupolar nuclei, such as ^{11}B, are quantitative when

Table 6. Summary of the Observed ^{11}B Resonances and Their Corresponding Assignments

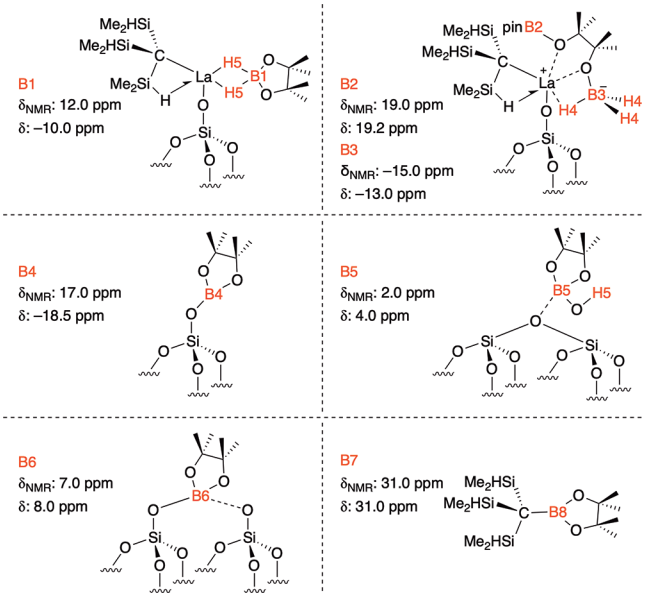

[a]Assignments for hydrogen in $-C(SiHMe_2)_3$ groups are shown in Figure 2A and Table 2. H1: $-SiH(CH_3)_2$; H2: $-SiH(CH_3)_2$; H3 is assigned to the methyl protons in HBpin derivatives. [b]Assignment for B7 (δ_{NMR} = −23.0 ppm, δ = −20.0 ppm) is unknown. δ_{NMR} and δ denote the observed NMR shift and "true" chemical shift, respectively, as explained in the text.

taken under appropriate experimental conditions (here, we used a small flip angle of 15° and rigorously confirmed that the recycle delay τ_{RD} was greater than $5T_1$ for all sites involved).[59] Thus, the spectra shown in Figure 5C,F,G reflect the relative abundance of each boron species in **1**@MSN_{550}+HBpin, **1**@MSN_{550}+HBpin reacted with acetophenone, and $(Me_2HSi)_3C-$Bpin@MSN_{550}, respectively. In contrast, the 2D spectra in Figure 5 are not quantitative but provide important structural information. The MQMAS experiment yields reliable values of ^{11}B chemical shifts for all species that it can detect,[60] which then may be referred to the solution-state NMR literature for specific assignments. Note that in the single quantum (SQ) dimension the quadrupolar interaction displaces the observed NMR shift of ^{11}B nucleus (δ_{NMR}) from "true" chemical shift (δ) by the so-called quadrupole induced shift (δ_{QIS}), whose contribution can be directly differentiated through the analysis of the MQMAS spectra.[60] Here, the contributions of δ_{QIS} are relatively small ($\leq$3 ppm) for all observed resonances (see Table 6). The relative peak intensities in the MQMAS spectra are skewed due to the strong dependence of the MQ excitation and conversion on the size of quadrupolar interaction and the local molecular motions.[61,62] The $^{1}H\{^{11}B\}$ HETCOR experiment relied on through-space $^{11}B \rightarrow {}^{1}H$ polarization transfers via heteronuclear dipolar couplings, which in turn depend on internuclear distances as well as molecular mobility. Under the experimental conditions used here (τ_{CP} = 0.2 ms), the observed $^{1}H-^{11}B$ correlations are dominated by short-range interactions. With this information in mind, we assigned the resonances labeled B1−B8 as follows.

B1, B2, and B3. The intense resonances labeled as B1, B2, and B3 are attributed to boron moieties associated with organolanthanide species. Specifically, B1 is assigned to the

https://dx.doi.org/10.1021/jacs.9b11606
J. Am. Chem. Soc. 2020, 142, 2935−2947

surface-attached lanthanum hydridopinacolborate, whereas B2 and B3 belong to the silica-bound borate-ring-opening pinacolborohydride zwitterionic structure formed by B1 further reacting with HBpin (Table 6). To support these assignments we first note that the chemical shifts for B2 and B3 extracted from the MQMAS spectrum (19.0 and −13.0 ppm, respectively) are close to the solution-state NMR values reported by Dudnik et al.[63] for the zwitterionic structure depicted in Figure 6A. Concurrently, hydrogen H4, which

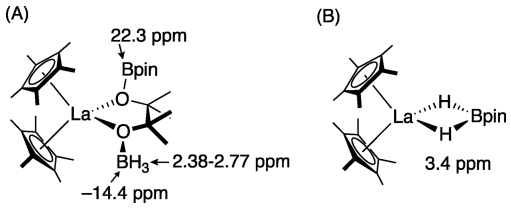

Figure 6. Structures of (A) the zwitterion formed by deactivating lanthanum hydride with HBpin and (B) the intermediate with two protons bridging boron and lanthanum, as proposed in ref 63.

shows strong correlation to B3 in the HETCOR spectrum (Figure 5B), resonates close to hydrogens in the $-OBH_3^-$ moiety in Figure 6A (1.9 ppm vs 2.38−2.77 ppm). According to Dudnik et al., the formation of the zwitterionic species occurs via lanthanum hydridopinacolborate intermediate $Cp^*_2La\{\mu^2-H_2Bpin\}$,[63] with two hydrogens bridging boron and lanthanum, as shown in Figure 6B. Since B1 correlates with H1, H3, and H5, and H5 has a chemical shift value (3.2 ppm) close to that of the two bridging protons (∼3.4 ppm, see Figure 6B), we assigned B1 to the analogous surface-bound lanthanum hydridopinacolborate (see Table 6). We could not independently verify the chemical shift for B1; however, the reported chemical shifts of boron dihydrides are higher than the corresponding trihydrides.[64] Based on previous studies, hydrogen H3, resonating at 0.9 ppm, can be unambiguously assigned to methyl groups of pinacolborane, whereas the assignment of H5 is discussed below.[39,65] Lastly, we note that the above assignments are consistent with the spectrum in Figure 5F, which demonstrates that the B1, B2, and B3 species were consumed during the catalytic reaction between **1**@MSN_{550}+HBpin and acetophenone (in the case of B2, this is less obvious due to the overlap with B4). We note that B1 is a proposed intermediate in the catalytic cycle for hydroboration of esters by $La\{C(SiHMe_2)_3\}_3$ under homogeneous conditions,[12] whereas the zwitterionic structure of B2/B3 corresponds to catalyst deactivation in hydroboration of pyridines.[63,66] The disappearance of B2 and B3 upon reaction with acetophenone suggests that the zwitterionic structure may transform back into an active species. This idea is consistent with the high catalytic activity of **1**@MSN_{700} for ketone hydroboration, which we measured to be 1000 turnovers within 5 min for the reaction of acetophenone.

B4, B5, and B6. The resonances labeled as B4, B5, and B6 appear to be associated with the reaction of HBpin with the silica surface. The structure corresponding to B4 was unambiguously established in our previous study.[39] Note that B4 overlaps with B2 in the ^{11}B DPMAS spectrum (Figure 5C); however, B4 is dominant. Sites B5 and B6 have not been previously observed. Based on the small second order quadrupolar broadening and the strong MQ intensity revealed by the MQMAS spectrum in Figure 5A, both of these sites are four-coordinated and are immobilized on the surface. Since resonance B6 correlates only with H3, we assigned it to the surface-attached −Bpin borate (i.e., four-oxygen coordination, see Table 6). B5, which correlates with H3 as well as H5 (3.2 ppm), is assigned to the silica-bound HOBpin. Indeed, according to Hwang et al., the OH resonance in three-oxygen coordinated boron is found at 3.3 ppm.[67] Accordingly, H5 has two contributions, the other one being the bridging proton between La and B1 (*vide supra*). Evidence for the assignments of B5 and B6 sites is also fortified by their chemical shifts.[68] We finally note that, upon the exposure of **1**@MSN_{550}+HBpin to acetophenone, B5 disappeared, suggesting that it reacted with the silica surface to form B4 or B6, both of which have indeed increased.

B7 and B8. The intensity of B7 is very small (see Figure 5C), and its existence mainly came to light in the MQMAS spectrum. B7 is likely involved in the catalytic process, since this peak disappeared when **1**@MSN_{550}+HBpin reacted with acetophenone (see Figure 5F); however, the experimental data are not sufficient for structural identification. B8, on the other hand, can be confidently assigned to $(Me_2HSi)_3C-Bpin$ that is weakly absorbed onto the silica surface. Since the boron resonance in $(Me_2HSi)_3C-Bpin$ is found at 32 ppm in solution-state NMR, we carried out the ^{11}B DPMAS measurement of $(Me_2HSi)_3C-Bpin$ adsorbed onto MSN_{550}. Indeed, the resulting spectrum (Figure 5G) is dominated by a peak at 31 ppm. The lack of B8 in the MQMAS and HETCOR spectra is consistent with the high molecular mobility. Note last that the spectrum in Figure 5G also includes resonances previously attributed to B4 and B5, which suggests that $(Me_2HSi)_3C-Bpin$ may react with surface hydroxyl groups in two different ways to generate B4, $(Me_2HSi)_3CH$, and HOBpin (B5), as illustrated in Scheme S3 in the Supporting Information.

Similarity between 1@MSN_{550}+HBpin and 1@MSN_{700}+HBpin. Whereas increasing the calcination temperature of MSN resulted in cleaner deposition of **1**, the ^{11}B DPMAS and MQMAS spectra of **1**@MSN_{550}+HBpin and **1**@MSN_{700}+HBpin showed the same set of resonances (see Figures S10 and S11 in the Supporting Information). The main observed change is in the relative peak intensities, with B5 and B6 being diminished compared to other peaks, which is consistent with the smaller surface concentration of SiOH groups.

CONCLUDING REMARKS

Tris(dimethylsilyl)methyl lanthanum compounds are effective precatalysts for ring-opening hydroboration of epoxides. The dimethylsilyl-based hydrocarbyl ligand provides a means for establishing the surface structures and coordination environment of supported electrophilic organolanthanide centers through spectroscopic analysis and comparisons with the homoleptic precursors. Importantly, the soluble species $La\{C(SiHMe_2)_3\}_3$ contains two bridging La←H−Si per alkyl ligand, whereas the monopodal grafted species contains only one La←H−Si per alkyl ligand. The number of La←H−Si in the complex reflects a combination of the electrophilicity and coordination number of the metal center, further perturbed by steric effects.

In $La\{C(SiHMe_2)_3\}_3$, the ligands are organized in an unusual approximate C_3 structure,[34] which is no longer possible in the surface-supported ≡Si—O—La$\{C(SiHMe_2)_3\}_2$. A comparison with related Ln←H—Si contain-

https://dx.doi.org/10.1021/jacs.9b11606
J. Am. Chem. Soc. 2020, 142, 2935−2947

ing species suggests that a combination of ≡Si—O—La and a Si—O—Si donor likely reduces the electrophilicity of the lanthanum center in ≡Si—O—La{C(SiHMe$_2$)$_3$}$_2$, as reflected by fewer La←H—Si per site. For example, zwitterionic Ce{C(SiHMe$_2$)$_3$}$_2$HB(C$_6$F$_5$)$_3$ and NdC(SiHMe$_2$)$_3${HB(C$_6$F$_5$)$_3$}$_2$ contain two Ln←H—Si per alkyl ligand as well as Ln←F and Ln←H—B in the coordination sphere.[69] The Nd complex features hexahapto toluene coordination.[70] These other ligands apparently do not interfere with the secondary interactions. In contrast, the $^1J_{Si-H}$ of surface-supported yttrium silazido species Y{N(SiHMe$_2$)*t*Bu}$_n$@MSN$_{700}$, which also contains Ln←H—Si, suggested a siloxane-based oxygen donor in addition to the surface ≡Si—O—Y interaction.[29]

These ≡Si—O—La{C(SiHMe$_2$)$_3$}$_2$ represent the preponderance of lanthanum sites grafted on the highly dehydroxylated surface, and accessing this uniformity was only possible by combination of ^{29}Si SSNMR spectroscopy with screening of grafting reactions conditions. Moreover, the detailed characterization of the sites, and the ability to prepare surface sites with high uniformity, facilitated the interrogation of catalytic properties through comparisons of solution phase and surface-organometallic performance.

Overall, the ≡Si—O—La{C(SiHMe$_2$)$_3$}$_2$ surface species performs equivalently or better than La{C(SiHMe$_2$)$_3$}$_3$ as a soluble catalyst for ring-opening hydroboration of epoxides, based on similar conversion times for equivalent mol % lanthanum in the reaction mixtures. This conclusion assumes that both soluble and supported catalytic sites activate equivalently, which is unlikely to be rigorously true. Likely, the kinetics and mechanisms of catalyst activation are distinct in these systems, and our current efforts are focused on probing these mechanisms through *in situ* spectroscopy in order to design supported catalysts with longer lifetimes and higher activities. The scrupulous ^{11}B SSNMR investigations that characterize the catalytic materials, postborylation, are a first, yet essential, step in this direction. Regardless, the total turnover numbers accessible for this recyclable, supported catalyst are significantly higher than the single-use soluble catalyst, which highlight the capacity of supported organolanthanum species in new catalytic transformations.

■ ASSOCIATED CONTENT

Supporting Information

The Supporting Information is available free of charge at https://pubs.acs.org/doi/10.1021/jacs.9b11606.

General experimental, synthesis and characterization of catalyst, catalytic hydroboration, and spectra (PDF)

■ AUTHOR INFORMATION

Corresponding Authors

Aaron D. Sadow − *Ames Laboratory, U.S. Department of Energy, Ames, Iowa 50011, United States; Department of Chemistry, Iowa State University, Ames, Iowa 50011, United States;* orcid.org/0000-0002-9517-1704; Email: sadow@iastate.edu

Marek Pruski − *Ames Laboratory, U.S. Department of Energy, Ames, Iowa 50011, United States; Department of Chemistry, Iowa State University, Ames, Iowa 50011, United States;* orcid.org/0000-0001-7800-5336; Email: mpruski@iastate.edu

Authors

Zhuoran Wang − *Ames Laboratory, U.S. Department of Energy, Ames, Iowa 50011, United States; Department of Chemistry, Iowa State University, Ames, Iowa 50011, United States*

Smita Patnaik − *Ames Laboratory, U.S. Department of Energy, Ames, Iowa 50011, United States; Department of Chemistry, Iowa State University, Ames, Iowa 50011, United States;* orcid.org/0000-0002-1210-1349

Naresh Eedugurala − *Ames Laboratory, U.S. Department of Energy, Ames, Iowa 50011, United States; Department of Chemistry, Iowa State University, Ames, Iowa 50011, United States;* orcid.org/0000-0003-4714-7993

J. Sebastián Manzano − *Ames Laboratory, U.S. Department of Energy, Ames, Iowa 50011, United States; Department of Chemistry, Iowa State University, Ames, Iowa 50011, United States;* orcid.org/0000-0003-2016-8380

Igor I. Slowing − *Ames Laboratory, U.S. Department of Energy, Ames, Iowa 50011, United States; Department of Chemistry, Iowa State University, Ames, Iowa 50011, United States;* orcid.org/0000-0002-9319-8639

Takeshi Kobayashi − *Ames Laboratory, U.S. Department of Energy, Ames, Iowa 50011, United States;* orcid.org/0000-0002-6366-0925

Complete contact information is available at: https://pubs.acs.org/10.1021/jacs.9b11606

Author Contributions

[§]Z.W. and S.P. contributed equally.

Notes

The authors declare no competing financial interest.

■ ACKNOWLEDGMENTS

The authors thank Dr. F.A. Perras for helpful discussions. This research was supported by the U.S. Department of Energy (DOE), Office of Science, Basic Energy Sciences, Division of Chemical Sciences, Geosciences, and Biosciences. The electron microscopy imaging was performed at the Sensitive Instrument Facility at Ames Laboratory, with the assistance of Dr. L. Zhou. Ames Laboratory is operated for the DOE by Iowa State University under Contract DE-AC02-07CH11358.

■ REFERENCES

(1) Watson, P. L.; Roe, D. C. β-Alkyl Transfer in a Lanthanide Model for Chain Termination. *J. Am. Chem. Soc.* **1982**, *104*, 6471−6473.

(2) Watson, P. L. Methane Exchange Reactions of Lanthanide and Early-transition-metal Methyl Complexes. *J. Am. Chem. Soc.* **1983**, *105*, 6491−6493.

(3) Watson, P. L.; Parshall, G. W. Organolanthanides in Catalysis. *Acc. Chem. Res.* **1985**, *18*, 51−56.

(4) Yang, F.; Libretto, N. J.; Komarneni, M. R.; Zhou, W.; Miller, J. T.; Zhu, X.; Resasco, D. E. Enhancement of m-Cresol Hydrodeoxygenation Selectivity on Ni Catalysts by Surface Decoration of MoO$_x$ Species. *ACS Catal.* **2019**, *9*, 7791−7800.

(5) Sergeev, A. G.; Webb, J. D.; Hartwig, J. F. A Heterogeneous Nickel Catalyst for the Hydrogenolysis of Aryl Ethers without Arene Hydrogenation. *J. Am. Chem. Soc.* **2012**, *134*, 20226−20229.

(6) Atesin, A. C.; Ray, N. A.; Stair, P. C.; Marks, T. J. Etheric C−O Bond Hydrogenolysis Using a Tandem Lanthanide Triflate/Supported Palladium Nanoparticle Catalyst System. *J. Am. Chem. Soc.* **2012**, *134*, 14682−14685.

(7) Sergeev, A. G.; Hartwig, J. F. Selective, Nickel-Catalyzed Hydrogenolysis of Aryl Ethers. *Science* **2011**, *332*, 439−443.

(8) Zhao, C.; Kou, Y.; Lemonidou, A. A.; Li, X.; Lercher, J. A. Highly Selective Catalytic Conversion of Phenolic Bio-Oil to Alkanes. *Angew. Chem.* **2009**, *121*, 4047−4050.
(9) Weidner, V. L.; Barger, C. J.; Delferro, M.; Lohr, T. L.; Marks, T. J. Rapid, Mild, and Selective Ketone and Aldehyde Hydroboration/Reduction Mediated by a Simple Lanthanide Catalyst. *ACS Catal.* **2017**, *7*, 1244−1247.
(10) Yan, D.; Dai, P.; Chen, S.; Xue, M.; Yao, Y.; Shen, Q.; Bao, X. Highly Efficient Hydroboration of Carbonyl Compounds Catalyzed by Tris(methylcyclopentadienyl)lanthanide Complexes. *Org. Biomol. Chem.* **2018**, *16*, 2787−2791.
(11) Chen, S.; Yan, D.; Xue, M.; Hong, Y.; Yao, Y.; Shen, Q. Tris(cyclopentadienyl)lanthanide Complexes as Catalysts for Hydroboration Reaction toward Aldehydes and Ketones. *Org. Lett.* **2017**, *19*, 3382−3385.
(12) Patnaik, S.; Sadow, A. D. Interconverting Lanthanum Hydride and Borohydride Catalysts for C=O Reduction and C−O Bond Cleavage. *Angew. Chem., Int. Ed.* **2019**, *58*, 2505−2509.
(13) Barger, C. J.; Motta, A.; Weidner, V. L.; Lohr, T. L.; Marks, T. J. La$[N(SiMe_3)_2]_3$-Catalyzed Ester Reductions with Pinacolborane: Scope and Mechanism of Ester Cleavage. *ACS Catal.* **2019**, *9*, 9015−9024.
(14) Song, H.; Ye, K.; Geng, P.; Han, X.; Liao, R.; Tung, C.-H.; Wang, W. Activation of Epoxides by a Cooperative Iron−Thiolate Catalyst: Intermediacy of Ferrous Alkoxides in Catalytic Hydroboration. *ACS Catal.* **2017**, *7*, 7709−7717.
(15) Desnoyer, A. N.; Geng, J.; Drover, M. W.; Patrick, B. O.; Love, J. A. Catalytic Functionalization of Styrenyl Epoxides via 2-Nickela(II)oxetanes. *Chem. - Eur. J.* **2017**, *23*, 11509−11512.
(16) He, X.; Hartwig, J. F. True Metal-Catalyzed Hydroboration with Titanium. *J. Am. Chem. Soc.* **1996**, *118*, 1696−1702.
(17) Oluyadi, A. A.; Ma, S.; Muhoro, C. N. Titanocene(II)-Catalyzed Hydroboration of Carbonyl Compounds. *Organometallics* **2013**, *32*, 70−78.
(18) Huang, Z.; Liu, D.; Camacho-Bunquin, J.; Zhang, G.; Yang, D.; López-Encarnación, J. M.; Xu, Y.; Ferrandon, M. S.; Niklas, J.; Poluektov, O. G.; Jellinek, J.; Lei, A.; Bunel, E. E.; Delferro, M. Supported Single-Site Ti(IV) on a Metal−Organic Framework for the Hydroboration of Carbonyl Compounds. *Organometallics* **2017**, *36*, 3921−3930.
(19) Ji, P.; Sawano, T.; Lin, Z.; Urban, A.; Boures, D.; Lin, W. Cerium-Hydride Secondary Building Units in a Porous Metal−Organic Framework for Catalytic Hydroboration and Hydrophosphination. *J. Am. Chem. Soc.* **2016**, *138*, 14860−14863.
(20) Anwander, R.; Runte, O.; Eppinger, J.; Gerstberger, G.; Herdtweck, E.; Spiegler, M. Synthesis and Structural Characterisation of Rare-earth Bis(dimethylsilyl)amides and Their Surface Organometallic Chemistry on Mesoporous MCM-41. *J. Chem. Soc., Dalton Trans.* **1998**, 847−858.
(21) Anwander, R.; Gorlitzer, H. W.; Gerstberger, G.; Palm, C.; Runte, O.; Spiegler, M. Grafting of Bulky Rare Earth Metal Complexes onto Mesoporous Silica MCM-41. *J. Chem. Soc., Dalton Trans.* **1999**, 3611−3615.
(22) Anwander, R. SOMC@PMS. Surface Organometallic Chemistry at Periodic Mesoporous Silica†. *Chem. Mater.* **2001**, *13*, 4419−4438.
(23) Fischbach, A.; Klimpel, M. G.; Widenmeyer, M.; Herdtweck, E.; Scherer, W.; Anwander, R. Stereospecific Polymerization of Isoprene with Molecular and MCM-48-grafted Lanthanide(III) Tetraalkylaluminates. *Angew. Chem., Int. Ed.* **2004**, *43*, 2234−2239.
(24) Gauvin, R. M.; Delevoye, L.; Hassan, R. A.; Keldenich, J.; Mortreux, A. Well-Defined Silica-Supported Rare-Earth Silylamides. *Inorg. Chem.* **2007**, *46*, 1062−1070.
(25) Le Roux, E.; Liang, Y.; Storz, M. P.; Anwander, R. Intramolecular Hydroamination/Cyclization of Aminoalkenes Catalyzed by Ln$[N(SiMe_3)_2]_3$ Grafted onto Periodic Mesoporous Silicas. *J. Am. Chem. Soc.* **2010**, *132*, 16368−16371.
(26) Conley, M. P.; Lapadula, G.; Sanders, K.; Gajan, D.; Lesage, A.; del Rosal, I.; Maron, L.; Lukens, W. W.; Copéret, C.; Andersen, R. A. The Nature of Secondary Interactions at Electrophilic Metal Sites of Molecular and Silica-Supported Organolutetium Complexes from Solid-State NMR Spectroscopy. *J. Am. Chem. Soc.* **2016**, *138*, 3831−3843.
(27) Ajellal, N.; Durieux, G.; Delevoye, L.; Tricot, G.; Dujardin, C.; Thomas, C. M.; Gauvin, R. M. Polymerization of Racemic β-Butyrolactone Using Supported Catalysts: A Simple Access to Isotactic Polymers. *Chem. Commun.* **2010**, *46*, 1032−1034.
(28) Liang, Y.; Anwander, R. Nanostructured Catalysts via Metal Amide-promoted Smart Grafting. *Dalton Trans.* **2013**, *42*, 12521−12545.
(29) Eedugurala, N.; Wang, Z.; Yan, K.; Boteju, K. C.; Chaudhary, U.; Kobayashi, T.; Ellern, A.; Slowing, I. I.; Pruski, M.; Sadow, A. D. β-SiH-Containing Tris(silazido) Rare-Earth Complexes as Homogeneous and Grafted Single-Site Catalyst Precursors for Hydroamination. *Organometallics* **2017**, *36*, 1142−1153.
(30) Bambirra, S.; Meetsma, A.; Hessen, B. Lanthanum Tribenzyl Complexes as Convenient Starting Materials for Organolanthanum Chemistry. *Organometallics* **2006**, *25*, 3454−3462.
(31) Hitchcock, P. B.; Lappert, M. F.; Smith, R. G.; Bartlett, R. A.; Power, P. P. Synthesis and Structural Characterization of the First Neutral Homoleptic Lanthanide Metal(III) Alkyls, $[LnR_3]$ [Ln = La or Sm, R = $CH(SiMe_3)_2$]. *J. Chem. Soc., Chem. Commun.* **1988**, 1007−1009.
(32) Vancompernolle, T.; Valente, A.; Chenal, T.; Zinck, P.; Del Rosal, I.; Maron, L.; Taoufik, M.; Harder, S.; Gauvin, R. M. Silica-Grafted Lanthanum Benzyl Species: Synthesis, Characterization, and Catalytic Applications. *Organometallics* **2017**, *36*, 3912−3920.
(33) Yan, K.; Pawlikowski, A. V.; Ebert, C.; Sadow, A. D. A Tris(alkyl)yttrium Compound Containing Six β-Agostic Si-H Interactions. *Chem. Commun.* **2009**, 656−658.
(34) Pindwal, A.; Yan, K.; Patnaik, S.; Schmidt, B. M.; Ellern, A.; Slowing, I. I.; Bae, C.; Sadow, A. D. Homoleptic Trivalent Tris(alkyl) Rare Earth Compounds. *J. Am. Chem. Soc.* **2017**, *139*, 16862−16874.
(35) Chabanas, M.; Quadrelli, E. A.; Fenet, B.; Coperet, C.; Thivolle-Cazat, J.; Basset, J.-M.; Lesage, A.; Emsley, L. Molecular Insight Into Surface Organometallic Chemistry Through the Combined Use of 2D HETCOR Solid-State NMR Spectroscopy and Silsesquioxane Analogs. *Angew. Chem., Int. Ed.* **2001**, *40*, 4493−4496.
(36) Le Roux, E.; Chabanas, M.; Baudouin, A.; de Mallmann, A.; Copéret, C.; Quadrelli, E. A.; Thivolle-Cazat, J.; Basset, J.-M.; Lukens, W.; Lesage, A.; Emsley, L.; Sunley, G. J. Detailed Structural Investigation of the Grafting of $[Ta(CH^tBu)(CH_2{}^tBu)_3]$ and $[Cp^*TaMe_4]$ on Silica Partially Dehydroxylated at 700 °C and the Activity of the Grafted Complexes toward Alkane Metathesis. *J. Am. Chem. Soc.* **2004**, *126*, 13391−13399.
(37) Blanc, F.; Basset, J.-M.; Copéret, C.; Sinha, A.; Tonzetich, Z. J.; Schrock, R. R.; Solans-Monfort, X.; Clot, E.; Eisenstein, O.; Lesage, A.; Emsley, L. Dynamics of Silica-Supported Catalysts Determined by Combining Solid-State NMR Spectroscopy and DFT Calculations. *J. Am. Chem. Soc.* **2008**, *130*, 5886−5900.
(38) Samantaray, M. K.; Alauzun, J.; Gajan, D.; Kavitake, S.; Mehdi, A.; Veyre, L.; Lelli, M.; Lesage, A.; Emsley, L.; Copéret, C.; Thieuleux, C. Evidence for Metal−Surface Interactions and Their Role in Stabilizing Well-Defined Immobilized Ru−NHC Alkene Metathesis Catalysts. *J. Am. Chem. Soc.* **2013**, *135*, 3193−3199.
(39) Eedugurala, N.; Wang, Z.; Chaudhary, U.; Nelson, N.; Kandel, K.; Kobayashi, T.; Slowing, I. I.; Pruski, M.; Sadow, A. D. Mesoporous Silica-Supported Amidozirconium-Catalyzed Carbonyl Hydroboration. *ACS Catal.* **2015**, *5*, 7399−7414.
(40) Aljuhani, M. A.; Barman, S.; Abou-Hamad, E.; Gurinov, A.; Ould-Chikh, S.; Guan, E.; Jedidi, A.; Cavallo, L.; Gates, B. C.; Pelletier, J. D. A.; Basset, J.-M. Imine Metathesis Catalyzed by a Silica-Supported Hafnium Imido Complex. *ACS Catal.* **2018**, *8*, 9440−9446.
(41) Gutmann, T.; Grünberg, A.; Rothermel, N.; Werner, M.; Srour, M.; Abdulhussain, S.; Tan, S.; Xu, Y.; Breitzke, H.; Buntkowsky, G. Solid-state NMR Concepts for the Investigation of Supported

https://dx.doi.org/10.1021/jacs.9b11606
J. Am. Chem. Soc. 2020, 142, 2935−2947

Transition Metal Catalysts and Nanoparticles. *Solid State Nucl. Magn. Reson.* **2013**, *55*−*56*, 1−11.
(42) Kandel, K.; Chaudhary, U.; Nelson, N. C.; Slowing, I. I. Synergistic Interaction between Oxides of Copper and Iron for Production of Fatty Alcohols from Fatty Acids. *ACS Catal.* **2015**, *5*, 6719−6723.
(43) Fujdala, K. L.; Tilley, T. D. An Efficient, Single-Source Molecular Precursor to Silicoaluminophosphates. *J. Am. Chem. Soc.* **2001**, *123*, 10133−10134.
(44) Lesage, A.; Emsley, L.; Chabanas, M.; Copéret, C.; Basset, J.-M. Observation of a H-Agostic Bond in a Highly Active Rhenium−Alkylidene Olefin Metathesis Heterogeneous Catalyst by Two-Dimensional Solid-State NMR Spectroscopy. *Angew. Chem., Int. Ed.* **2002**, *41*, 4535−4538.
(45) Medek, A.; Harwood, J. S.; Frydman, L. Multiple-Quantum Magic-Angle Spinning NMR: A New Method for the Study of Quadrupolar Nuclei in Solids. *J. Am. Chem. Soc.* **1995**, *117*, 12779−12787.
(46) Ishii, Y.; Tycko, R. Sensitivity Enhancement in Solid State ^{15}N NMR by Indirect Detection with High-Speed Magic Angle Spinning. *J. Magn. Reson.* **2000**, *142*, 199−204.
(47) Wiench, J. W.; Bronnimann, C. E.; Lin, V. S. Y.; Pruski, M. Chemical Shift Correlation NMR Spectroscopy with Indirect Detection in Fast Rotating Solids: Studies of Organically Functionalized Mesoporous Silicas. *J. Am. Chem. Soc.* **2007**, *129*, 12076−12077.
(48) Harris, R. K.; Becker, E. D.; Cabral de Menezes, S. M.; Granger, P.; Hoffman, R. E.; Zilm, K. W. Further Conventions for NMR Shielding and Chemical Shifts (IUPAC Recommendations 2008). *Pure Appl. Chem.* **2008**, *80*, 59.
(49) Kandel, K.; Frederickson, C.; Smith, E. A.; Lee, Y.-J.; Slowing, I. I. Bifunctional Adsorbent-Catalytic Nanoparticles for the Refining of Renewable Feedstocks. *ACS Catal.* **2013**, *3*, 2750−2758.
(50) Parkin, G. 1.01—Classification of Organotransition Metal Compounds. In *Comprehensive Organometallic Chemistry III*; Mingos, D. M. P., Crabtree, R. H., Eds.; Elsevier: Oxford, 2007; pp 1−57.
(51) Tuel, A.; Hommel, H.; Legrand, A. P.; Kovats, E. S. A Silicon-29 NMR Study of the Silanol Population at the Surface of Derivatized Silica. *Langmuir* **1990**, *6*, 770−775.
(52) Liu, S. F.; Mao, J. D.; Schmidt-Rohr, K. A Robust Technique for Two-Dimensional Separation of Undistorted Chemical-Shift Anisotropy Powder Patterns in Magic-Angle-Spinning NMR. *J. Magn. Reson.* **2002**, *155*, 15−28.
(53) Radu, N. S.; Hollander, F. J.; Tilley, T. D.; Rheingold, A. L. Samarium-mediated Redistribution of Silanes and Formation of Trinuclear Samarium-Silicon Clusters. *Chem. Commun.* **1996**, 2459−2460.
(54) Castillo, I.; Tilley, T. D. Organolutetium Complexes in σ-Bond Metathesis Reactions Involving Silicon. Catalysts for the Hydrogenolysis of Si-C Bonds. *Organometallics* **2001**, *20*, 5598−5605.
(55) Basset, J.-M.; Lefebvre, F.; Santini, C. Surface Organometallic Chemistry: Some Fundamental Features Including the Coordination Effects of the Support. *Coord. Chem. Rev.* **1998**, *178*−*180*, 1703−1723.
(56) Vinogradov, E.; Madhu, P. K.; Vega, S. High-resolution Proton Solid-state NMR Spectroscopy by Phase-modulated Lee−Goldburg Experiment. *Chem. Phys. Lett.* **1999**, *314*, 443−450.
(57) Rataboul, F.; Baudouin, A.; Thieuleux, C.; Veyre, L.; Copéret, C.; Thivolle-Cazat, J.; Basset, J.-M.; Lesage, A.; Emsley, L. Molecular Understanding of the Formation of Surface Zirconium Hydrides upon Thermal Treatment under Hydrogen of $[(\equiv SiO)Zr(CH_2tBu)_3]$ by Using Advanced Solid-State NMR Techniques. *J. Am. Chem. Soc.* **2004**, *126*, 12541−12550.
(58) Eaborn, C.; Hitchcock, P. B.; Lickiss, P. D. Some Derivatives of Tris(Dimethylsilyl)Methane - a Novel Bicyclic Tris(Disiloxane) with a Manaxane Structure. *J. Organomet. Chem.* **1983**, *252*, 281−288.
(59) Freude, D.; Haase, J. Quadrupole Effects in Solid-State Nuclear Magnetic Resonance. In *NMR Basic Principles and Progress: Special Applications*; Pfeifer, H., Barker, P., Eds.; Springer: Berlin, 1993; pp 1−90.
(60) Fernandez, C.; Pruski, M. Probing Quadrupolar Nuclei by Solid-State NMR Spectroscopy: Recent Advances. In *Solid State NMR*; Chan, J. C. C., Ed.; Springer: Berlin, 2012; Vol. *306*, pp 119−188.
(61) Amoureux, J.-P.; Fernandez, C.; Frydman, L. Optimized Multiple-quantum Magic-angle Spinning NMR Experiments on Half-integer Quadrupoles. *Chem. Phys. Lett.* **1996**, *259*, 347−355.
(62) Kotecha, M.; Chaudhuri, S.; Grey, C. P.; Frydman, L. Dynamic Effects in MAS and MQMAS NMR Spectra of Half-Integer Quadrupolar Nuclei: Calculations and an Application to the Double Perovskite Cryolite. *J. Am. Chem. Soc.* **2005**, *127*, 16701−16712.
(63) Dudnik, A. S.; Weidner, V. L.; Motta, A.; Delferro, M.; Marks, T. J. Atom-efficient Regioselective 1,2-Dearomatization of Functionalized Pyridines by an Earth-abundant Organolanthanide Catalyst. *Nat. Chem.* **2014**, *6*, 1100−1107.
(64) Kemmitt, T.; Gainsford, G. J. Regeneration of Sodium Borohydride from Sodium Metaborate, and Isolation of Intermediate Compounds. *Int. J. Hydrogen Energy* **2009**, *34*, 5726−5731.
(65) Tucker, C. E.; Davidson, J.; Knochel, P. Mild and Stereoselective Hydroborations of Functionalized Alkynes and Alkenes Using Pinacolborane. *J. Org. Chem.* **1992**, *57*, 3482−3485.
(66) Hill, M. S.; Kociok-Kohn, G.; MacDougall, D. J.; Mahon, M. F.; Weetman, C. Magnesium Hydrides and the Dearomatisation of Pyridine and Quinoline Derivatives. *Dalton Trans.* **2011**, *40*, 12500−12509.
(67) Hwang, S.-J.; Chen, C.-Y.; Zones, S. I. Boron Sites in Borosilicate Zeolites at Various Stages of Hydration Studied by Solid State NMR Spectroscopy. *J. Phys. Chem. B* **2004**, *108*, 18535−18546.
(68) Henderson, W. G.; How, M. J.; Kennedy, G. R.; Mooney, E. F. The Interconversion of Aqueous Boron Species and the Interaction of Borate with Diols: A ^{11}B NMR Study. *Carbohydr. Res.* **1973**, *28*, 1−12.
(69) Pindwal, A.; Patnaik, S.; Everett, W. C.; Ellern, A.; Windus, T. L.; Sadow, A. D. Cerium-Catalyzed Hydrosilylation of Acrylates to Give α-Silyl Esters. *Angew. Chem., Int. Ed.* **2017**, *56*, 628−631.
(70) Schmidt, B. M.; Pindwal, A.; Venkatesh, A.; Ellern, A.; Rossini, A. J.; Sadow, A. D. Zwitterionic Trivalent (Alkyl)lanthanide Complexes in Ziegler-Type Butadiene Polymerization. *ACS Catal.* **2019**, *9*, 827−838.

https://dx.doi.org/10.1021/jacs.9b11606
J. Am. Chem. Soc. 2020, 142, 2935−2947